

# Insight into the SBU Condensation in Mg Coordination and Supramolecular Frameworks: A Combined Experimental and Theoretical Study

Ana E. Platero-Prats,<sup>†</sup> Víctor A. de la Peña-O'Shea,<sup>‡</sup> Davide M. Proserpio,<sup>§</sup> Natalia Snejko,<sup>†</sup> Enrique Gutiérrez-Puebla,<sup>\*,†</sup> and Ángeles Monge<sup>\*,†</sup>

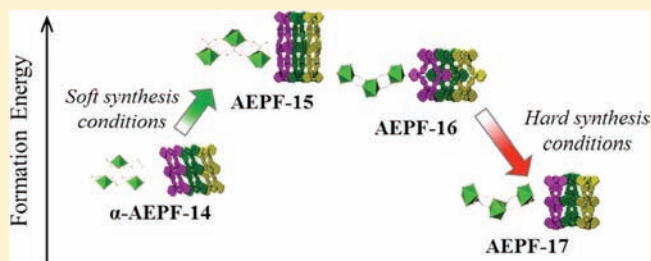
<sup>†</sup>Department of New Architectures in Materials Chemistry, Instituto de Ciencia de Materiales de Madrid, ICMM-CSIC, c/Sor Juana Inés de la Cruz, 3, 28049 Madrid, Spain

<sup>‡</sup>Thermochemical Process Group, Instituto Madrileño de Estudios Avanzados en Energía (IMDEA Energía), Avenida Ramón de la Sagra n° 3 28935 Móstoles, Spain

<sup>§</sup>Dipartimento di Chimica Strutturale e Stereochimica Inorganica, Università degli studi di Milano, via G. Venezian 21, 20133 Milano, Italy

## Supporting Information

**ABSTRACT:** This work is to emphasize the influence of the synthetic procedures in the isolation of different coordination polymers that coexist under hydro-/solvothetical conditions. An experimental and theoretical study in the Mg<sup>2+</sup>:4,4'-(hexafluoroisopropylidene)bis(benzoic acid):1,10-phenanthroline system has been carried out. Computational studies have determined the relative energies for those compounds that coexist under certain hydrothermal conditions, and have helped to identify the driving forces for the formation of the different phases. The five new compounds belong to five different structural types: **AEPF-14**, which presents two polymorphs ( $\alpha$ - and  $\beta$ -) ( $[\text{Mg}(\text{H}_2\text{O})_4(\text{phen})_2]\text{L}$ ), **AEPF-15** ( $[\text{Mg}(\text{HL})_2(\text{phen})]$ ) and **AEPF-16** ( $[\text{Mg}(\text{H}_2\text{O})_2(\text{L})(\text{phen})]$ ) are both 1D MOFs (**AEPF-16** with a helical structure), and **AEPF-17** ( $[\text{Mg}(\text{H}_2\text{O})(\text{L})(\text{phen})]$ ) with a 2D structure. Hydrogen bond interactions found in the five compounds have been taken into account to study the topology of their supramolecular nets. Finally, dehydration studies performed on **AEPF-14** ( $\alpha$ - and  $\beta$ -) and **AEPF-16** have shown that the topological type of their supramolecular networks determines the structural changes that take place during the dehydration processes of these Mg compounds.



## INTRODUCTION

The current environmental needs, which are becoming more and more considered in chemistry research, have posed new scientific challenges. In this sense, obtaining new structural types by using alkaline-earth elements (AE) could represent a comparatively cheap, nontoxic, and green alternative to conventional MOFs, which are mostly based on transition metals or, more recently, rare-earth elements. However, despite these advantages, the synthesis of AE-MOFs still remains much less explored, mainly due to the inherent difficulties arising from these elements such as their formation/crystallization processes, their unpredictable coordination numbers and geometries, and the tendency of these elements to form solvated species.<sup>1</sup> The recent efforts made in such a way have given rise to different exciting novel AE-MOFs with good performances in gas/liquid separations<sup>2</sup> or heterogeneous catalysis,<sup>3</sup> proving the viability of this green alternative.

Besides the choice of the metal ion, the type of ligand (geometry, number/relative position of functional groups, flexibility) is crucial in the formation of new nets. Moreover, the choice of flexible ligands can induce some additional interesting structural features, like reversible phase transitions<sup>2b</sup>

or polymorphism phenomena.<sup>4</sup> The insertion of ancillary ligands in the synthesis media is usually an approach to control the framework connectivity, and in this case could minimize the Mg solvation.

Continuing our research on AE-MOFs,<sup>2b,5</sup> here we report the synthesis, crystal structures, and characterization of five novel Alkaline-Earth Polymeric Frameworks (AEPF) based on magnesium, (hexafluoroisopropylidene)bis(benzoic acid) ( $\text{H}_2\text{L}$ , from now on), and 1,10-phenanthroline (phen, from now on) ligands. These five AEPFs exhibit 0D, 1D, and 2D dimensionalities, and 2D and 3D supramolecular frameworks: a molecular magnesium material with polymorphism (named **AEPF-14**,  $\alpha$ - and  $\beta$ -phases,  $[\text{Mg}(\text{H}_2\text{O})_4(\text{phen})_2]\text{L}$ ), a 1D MOF (**AEPF-15**,  $[\text{Mg}(\text{HL})_2(\text{phen})]$ ), a 1D helical MOF (**AEPF-16**,  $[\text{Mg}(\text{H}_2\text{O})_2(\text{L})(\text{phen})]$ ), and a 2D MOF (**AEPF-17**,  $[\text{Mg}(\text{H}_2\text{O})(\text{L})(\text{phen})]$ ). The role that the synthesis conditions play in the formation of each phase has been extensively studied. Moreover, a combination of topological comparative analyses

Received: November 10, 2011

Published: February 21, 2012

with computational studies has been performed to determine the relative energies for the five obtained networks.

The aim of this work is to emphasize the high significance of fine-tuning the synthetic procedure to obtain each magnesium compound a separated phase under hydro- or solvothermal conditions, and to theoretically study the relative energies for those compounds that coexist under certain hydrothermal conditions, knowing in this way the thermodynamic or kinetic control that drives each reaction.

## EXPERIMENTAL SECTION

**General Information.** All reagents were purchased at high purity (AR grade) and used without further purification. IR spectra were recorded from KBr pellets in the range 4000–400  $\text{cm}^{-1}$  on a Nicolet FT-IR 20SXC spectrometer (see the Supporting Information, Section S4). Thermogravimetric thermal analyses (TGA) were performed with a SEIKO model EXSTAR 6300 apparatus in the temperature range between 25 and 850  $^{\circ}\text{C}$  (Ar flow rate 50  $\text{mL}\cdot\text{min}^{-1}$ ) (see the Supporting Information, Section S5).

**Synthesis Procedures.** The five compounds presented in this work (named  $\alpha$ -AEPF-14,  $\beta$ -AEPF-14, AEPF-15, AEPF-16, and AEPF-17) were synthesized under hydro- or solvothermal conditions. After optimizing the synthetic procedures, it was possible to obtain all these compounds (except for AEPF-15) as pure crystalline phases. For the best reaction conditions determined in each case see the Supporting Information (Section S1).

**Structure Determination by Single Crystal X-ray Diffraction.** Suitable crystals of  $\alpha$ -AEPF-14,  $\beta$ -AEPF-14, AEPF-15, AEPF-16, and AEPF-17 were selected under a polarizing optical microscope and were glued on a glass fiber. Data were collected at 298 K on a Bruker four circle  $\kappa$ -diffractometer equipped with a Cu microsource operated at 30 W power (45 kV, 0.60 mA) to generate Cu  $K\alpha$  radiation ( $\lambda = 1.54178 \text{ \AA}$ ), and a Bruker AXIOM area detector (microgap technology) ( $\beta$ -AEPF-14 and AEPF-16) or an Bruker APEXII area detector ( $\alpha$ -AEPF-14, AEPF-15, and AEPF-17); exploring over a hemisphere of the reciprocal space in a combination of  $\varphi$  and  $\omega$  scans, using a Bruker APEX2 software suite. Unit cell dimensions were determined by a least-squares fit of reflections with  $I > 2\sigma(I)$ . Data were then integrated and scaled by using the SAINTplus<sup>6</sup> program. Semiempirical absorption and scale corrections based on equivalent reflections were carried out with SADABS.<sup>7</sup> Space group determinations and tests for merohedral twinning were carried out with XPREP.<sup>8</sup> The structures were solved by using the Direct Methods program SHELXS.<sup>8</sup> The final cycles of refinement were carried out by full-matrix least-squares analyses with anisotropic thermal parameters for all non-hydrogen atoms. All hydrogen atoms were placed in geometrically calculated positions and subsequently refined by using a riding model with  $U_{\text{iso}}(\text{H}) = 1.2U_{\text{eq}}(\text{C})$ , except for those of water molecules, which were located from difference Fourier maps. The final structures were examined and tested by using PLATON.<sup>9</sup> CCDC reference numbers CCDC 847926–847930 contain the supplementary crystallographic data for this paper. These data can be obtained free of charge from the Cambridge Crystallographic Data Center.

**Powder X-ray Diffraction.** Powder X-ray Diffraction (PXRD) measurements were performed with a Bruker D8 diffractometer in the  $\theta$ – $\theta$  mode, using nickel-filtered Cu  $K\alpha_{1,2}$  ( $\lambda = 0.15418 \text{ nm}$ ) radiation. The best counting statistics were achieved by using a scanning step of 0.02 $^{\circ}$  between 5 $^{\circ}$  and 35 $^{\circ}$  Bragg angles with an exposure time of 0.5 s per step. Pawley refinements<sup>10</sup> were performed by using Materials Studio software<sup>11</sup> for those compounds presented in this work that have been obtained as pure phases.

**Topological Analyses.** The topological analyses of the AEPFs presented in this work were performed with TOPOS software<sup>12</sup> following the principle of underlying nets.<sup>13,14</sup> In all cases, hydrogen bond interactions were taken into account to study the topology of supramolecular frameworks.

**Computational Details.** The structural stability ab initio calculations of the five compounds presented in this work have been

carried out by periodic Density Functional Theory (DFT). The DFT plane-wave calculations were realized by using the VASP package.<sup>15,16</sup> The total energy was computed by using the revised Perdew-Burke-Ernzerhof GGA<sup>17,18</sup> exchange-correlation function. The effect of the core electrons on the valence electron density was described by the projector augmented wave (PAW) method.<sup>19,20</sup> The cutoff for the kinetic energy of the plane-waves has been set to 415 eV throughout, which after extensive test proved to ensure a total energy convergence better than 10<sup>–5</sup> eV. Geometry optimization on selected starting geometries obtained from single crystal X-ray diffraction was carried out by using a gradient-conjugate method. The apparent formation energy was calculated as an energy difference between the corresponding reagents and MOFs products.

## RESULTS AND DISCUSSION

**Effect of Synthesis Conditions.** In this work five new magnesium compounds based on the flexible H<sub>2</sub>L dicarboxylate linker and the ancillary chelating N-donor phen ligand are going to be discussed from the structural, energetic stability, and topological point of view. The high number of obtained compounds proves that a wide variety of supramolecular frameworks can be obtained starting from the same primary building units (that is, octahedral Mg<sup>2+</sup> ions as metallic centers and H<sub>2</sub>L and phen as ligands). The aim of this work is to emphasize the high influence of the synthetic procedure terms on the formation of each of these magnesium compounds under hydro- or solvothermal conditions. The experiments performed during this investigation not only have led to isolation of the highest number of compounds, but also to understanding the influence of the experimental variables involved in the formation of each magnesium framework.

The hydrothermal reaction of magnesium acetate tetrahydrate and H<sub>2</sub>L with phen as chelating ligand at 160  $^{\circ}\text{C}$  during 2 days gave rise to a heterogeneous crystalline product (the composition of the reaction mixture was 1 Mg<sup>2+</sup>:1 phen:1 H<sub>2</sub>L molar ratio). After careful analysis of this product, single crystals with different morphologies were identified and their crystal structures were solved by single crystal X-ray diffraction experiments, which corresponded to different novel magnesium compounds:  $\alpha$ -AEPF-14 ([Mg(H<sub>2</sub>O)<sub>4</sub>(phen)]L), AEPF-15 ([Mg(HL)<sub>2</sub>(phen)]), and AEPF-16 ([Mg(H<sub>2</sub>O)<sub>2</sub>(L)(phen)]). With the aim of obtaining these three compounds as pure crystalline phases, a rational optimization of the hydrothermal synthesis conditions (SC), was carried out (Table 1). The effect

**Table 1.** Explored Hydrothermal Synthesis Conditions on the System 1 Mg<sup>2+</sup>:1 phen:1 H<sub>2</sub>L

SC	T ( $^{\circ}\text{C}$ )	time	pH	phase
1	160	1 h	6	$\alpha$ -AEPF-14
2	160	2 h	6	$\alpha$ -AEPF-14 > AEPF-15, AEPF-16
3	160	3 h	6	$\alpha$ -AEPF-14 > AEPF-15, AEPF-16
4	160	2 days	6	AEPF-15 > $\alpha$ -AEPF-14, AEPF-16
5	170	1 h	6	$\alpha$ -AEPF-14, AEPF-15
6	170	2 h	6	AEPF-15 $\gg$ AEPF-16
7	170	3 h	6	AEPF-15 $\gg$ AEPF-16
8	170	2 days	6	AEPF-15 $\gg$ AEPF-16
9	180	1 day	6	AEPF-16, AEPF-17
10	180	5 days	6	AEPF-17 > AEPF-16
11	180	10 days	6	AEPF-17 > AEPF-16
12	180	1 days	7	AEPF-16 > AEPF-17
13	180	5 days	7	AEPF-16
14	180	10 days	7	AEPF-16
15	200	1 day	6	AEPF-16 > AEPF-17
16	200	5 days	6	AEPF-16, AEPF-17
17	200	10 days	6	AEPF-17 > AEPF-16

of the reaction temperature and time (without changes in the composition of the reaction mixture) was systematically studied and the main results are discussed in the following.

In a first step, kinetic parameters (without temperature changes) were evaluated (Table 1, SC1–SC4), showing the formation of  $\alpha$ -AEPF-14 compound as a pure phase when short reaction times are used (1 h) (SC1). The increase of reaction time up to 2 and then to 3 h (SC2 and SC3, respectively) gave rise to a mixture of  $\alpha$ -AEPF-14, AEPF-15, and AEPF-16 in which  $\alpha$ -AEPF-14 was the principal component. The proportion of this mixture changed after 2 days of reaction, when AEPF-15 compound became the principal component of the mixture (SC4).

In order to study the thermodynamic effects, a series of reactions were also performed increasing the reaction temperature up to 170 °C (Table 1, SC5–SC8). Thus, when short reaction times are used (1 h), a mixture of  $\alpha$ -AEPF-14 and AEPF-15 was determined (SC5) (~50% of each phase). An increase of the reaction time up to 2 and then to 3 h (SC6 and SC7) led to a crystalline mixture for which the main component was AEPF-15, together with traces of AEPF-16. The same result was obtained after increasing the time of reaction up to 2 days (SC8).

Taking into account the important role that both the thermodynamic and the kinetic effects play, several experiments were then performed at a higher temperature (180 °C) and longer reaction times (1, 5, and 10 days) (Table 1, SC9–SC11). Under these hydrothermal conditions, when the time of reaction was 1 day, a mixture of AEPF-16 and a new phase named AEPF-17 was obtained (~50% of each) (SC9). Increasing the reaction time up to 5 and 10 days (SC10 and SC11), the contribution of AEPF-17 in the mixture increased. However, it was not possible to obtain either of the two compounds as pure phases.

At this point, the pH was also considered as an additional variable. Thus, in the next step, the effect of the pH increasing up to 7 by using a NaOH solution (0.1 M) was investigated (Table 1, SC12–SC14). By comparison of the sample obtained after 1 day of reaction at pH 7 (SC12) to that obtained at pH 6 (SC9), it could be concluded that a higher pH value favors the formation of AEPF-16 instead of AEPF-17. Finally, at longer time periods (5 and 10 days) (SC13–SC14), AEPF-16 was successfully isolated.

Once the AEPF-16 compound was synthesized as a pure phase, several experiments were carried out to establish the reaction conditions under which AEPF-17 could be isolated. With this propose, a series of hydrothermal reactions were performed to evaluate the effect of a higher temperature (200 °C) (Table 1, SC15–SC17). Thus, after 1 day of reaction, a mixture of AEPF-16 (major component) and AEPF-17 was obtained (SC15). When longer reaction times are used, AEPF-17 became the principal mixture component (SC16–SC17). However, yet under these conditions it was not possible to isolate AEPF-17.

Taking into account the unsuccessful efforts to purify the AEPF-17 phase under high-temperature hydrothermal conditions (200 °C), we then introduced changes in the polarity of the reaction media. For that purpose, a mixture of acetone ( $\text{Me}_2\text{CO}$ ) and water was chosen as solvent media, using different volume ratios (Table 2). It is worth mentioning that, although a wide variety of conditions were investigated during this work (the studied variables were as follows: time, temperature, and  $\text{H}_2\text{O}:\text{Me}_2\text{CO}$  volume ratio), at the beginning all the experiments resulted in the formation of liquids. Moreover, during the development of this investigation it was

observed that the heating rate played an important role. Up to the moment, all the experiments were performed placing the

**Table 2. Explored Solvothermal Synthesis Conditions on the System 1  $\text{Mg}^{2+}:\text{1 phen}:\text{1 H}_2\text{L}$**

SC	$T$ (°C)	time (days)	$\text{H}_2\text{O}:\text{Me}_2\text{CO}$	phase	heating
16	200	5	1:0	AEPF-16, AEPF-17	fast
18	200	5	1:0	$\beta$ -AEPF-14, amorphous	slow
19	200	5	20:1	AEPF-17	slow
20	200	5	5:1	amorphous	slow
21	200	5	2:1	$\beta$ -AEPF-14	slow
22	200	5	1:1	$\beta$ -AEPF-14	slow
23	200	5	1:5	liquid	slow
24	200	5	0:1	liquid	slow

autoclave reactors in a preheated oven at the desired temperatures (fast heating, SC16). However, in this case, certain hydrothermal conditions were chosen and the reaction was then repeated by using a slow heating treatment ( $5\text{ °C}\cdot\text{min}^{-1}$ , slow heating, SC18). Surprisingly, under this slow heating condition, a new compound was determined (named  $\beta$ -AEPF-14, which is a polymorph of  $\alpha$ -AEPF-14), together with an important amorphous contribution. Taking into account this interesting result, an optimization of solvothermal conditions was carried out by using slow heating treatments ( $T = 200\text{ °C}$  and 5 days reaction time), systematically varying the polarity of the reaction media ( $\text{H}_2\text{O}:\text{Me}_2\text{CO}$  volume ratio). The main results are presented in Table 2.

Thus, a decrease in the polarity ( $\text{H}_2\text{O}:\text{Me}_2\text{CO}$  volume ratios = 2:1 and 1:1) led to the successful formation of  $\beta$ -AEPF-14 as a pure phase (SC21 and SC22). In addition, at higher  $\text{H}_2\text{O}:\text{Me}_2\text{CO}$  volume ratio of 20:1, AEPF-17 was also synthesized as a pure phase (SC19). Finally, when the mixture is mainly or totally composed by  $\text{Me}_2\text{CO}$  (SC23 and SC24), the solvothermal reactions resulted in the formation of liquids.

To summarize all the above-mentioned results, after rationally optimizing the synthesis procedures: (i) Two AEPF-14 polymorphs were obtained as pure crystalline phases under hydrothermal conditions ( $\alpha$ -phase, SC1) and solvothermal conditions ( $\beta$ -phase, SC21) varying the polarity media; (ii) In addition, AEPF-16 compound was isolated by increasing the pH (SC13). (iii) AEPF-17 (as it occurs for  $\beta$ -AEPF-14) is obtained as a pure crystalline phase under solvothermal conditions, using slow heating treatments (SC19). Schemes 1 and 2 summarize the synthesis optimization procedures carried out under hydrothermal and solvothermal conditions, respectively, to obtain each new magnesium phase.

**Crystal Structure Description and Topological Analyses.** Details of the single crystal X-ray diffraction data collection, cell parameters, and crystal structure refinement for the five compounds presented in this work are given in Tables S1–S5 (Supporting Information). The corresponding ORTEP representations for these crystal structures are shown in Figures S1–S5 (Supporting Information). A summary of the structural and topological features for AEPF-14 ( $\alpha$ - and  $\beta$ -), AEPF-15, AEPF-16, and AEPF-17 are depicted in Figure 1. Details about the topological simplifications carried out are shown in Figure 2.

**AEPF-14 Polymorphs.** The  $[\text{Mg}(\text{H}_2\text{O})_4(\text{phen})]\text{L}$  compound (AEPF-14) presents two different polymorphs, named  $\alpha$ - and  $\beta$ -phases, which were isolated under hydro- and

Scheme 1. Summary of the Explored Hydrothermal Synthesis Conditions

160 °C	$\alpha$ -AEPF-14	$\alpha$ -AEPF-14 > AEPF-15, AEPF-16	AEPF-15 > $\alpha$ -AEPF-14, AEPF-16	pH= 6
170 °C	$\alpha$ -AEPF-14, AEPF-15	AEPF-15 >> AEPF-16	AEPF-15 >> AEPF-16	pH= 6
		1h	2 days	
Time				
180 °C	AEPF-16, AEPF-17	AEPF-17 > AEPF-16	AEPF-17 > AEPF-16	pH= 6
180 °C	AEPF-16 > AEPF-17	AEPF-16	AEPF-16	pH=7
200 °C	AEPF-16 > AEPF-17	AEPF-16, AEPF-17	AEPF-17 > AEPF-16	pH=6
		1day	10 days	
Time				

Scheme 2. Summary of the Studied Solvothermal Synthesis Conditions

200°C	$\beta$ -AEPF-14, amorphous	AEPF-17	$\beta$ -AEPF-14
	1:0	20:1	2:1
	H <sub>2</sub> O		Me <sub>2</sub> CO

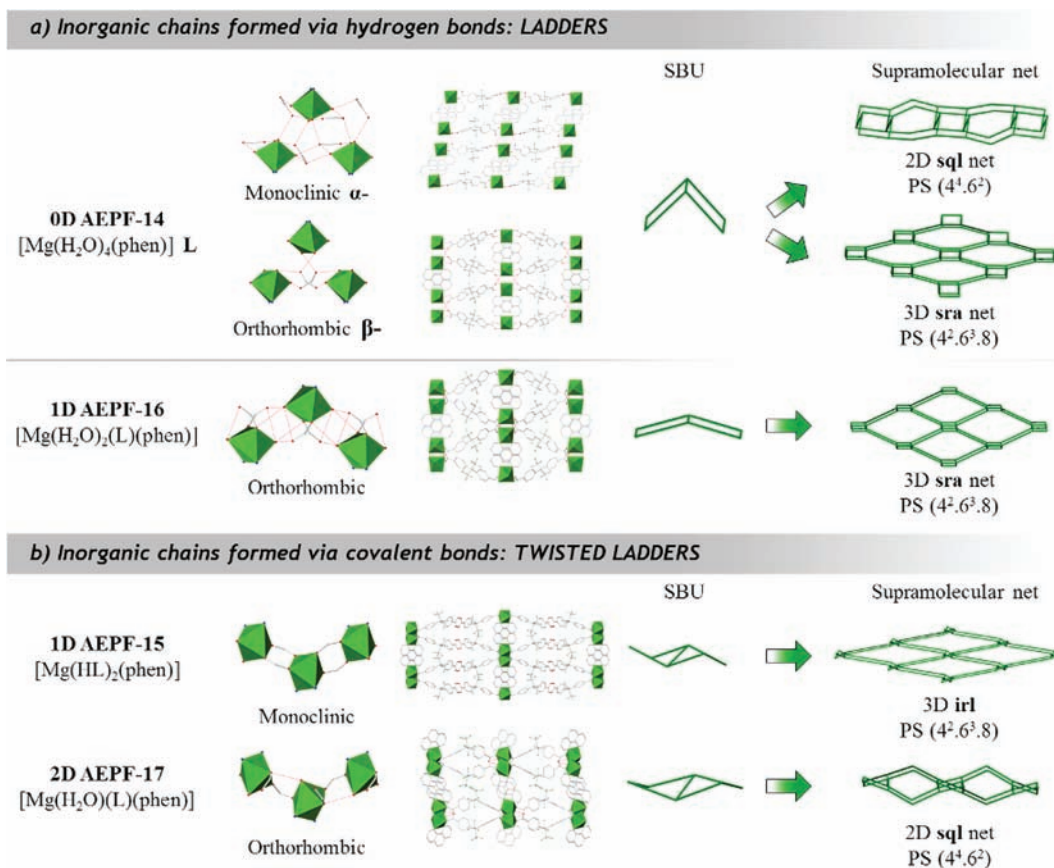


**Figure 1.** Summary of the structural and topological features of compounds in which inorganic chains are formed (a) via hydrogen bonds (AEPF-14 ( $\alpha$ - and  $\beta$ -phases) and AEPF-16) and (b) via covalent bonds (AEPF-15 and AEPF-17). Hydrogen bonds determined in these materials are depicted in red.

Table 3. Summary of the Structure Parameters Determined for AEPF-14 Polymorphs

AEPF-14	$\alpha$ -phase	$\beta$ -phase
empirical formula	$C_{29}H_{24}F_6MgN_2O_8$	
formula weight	666.81	
wavelength	1.54178 Å	
crystal system	monoclinic	orthorhombic
space group	$P2_1/c$	$Pnna$
unit cell dimensions	$a = 13.2022(2)$ Å $b = 7.6135(1)$ Å $c = 31.0128(5)$ Å	$a = 7.3064(2)$ Å $b = 32.602(1)$ Å $c = 12.5442(4)$ Å
volume	$3071.18(8)$ Å <sup>3</sup>	$2988.11(16)$ Å <sup>3</sup>
Z	4	4
independent reflcns	4821 [R(int) = 0.0296]	2434 [R(int) = 0.0726]
data/restraints/parameters	4821/8/447	2434/4/226
goodness-of-fit on $F^2$	1.035	1.055
final R indices [ $I > 2\sigma(I)$ ]	$R_1 = 0.0464$ , $wR_2 = 0.1191$	$R_1 = 0.0460$ , $wR_2 = 0.1261$
R indices (all data)	$R_1 = 0.0650$ , $wR_2 = 0.1322$	$R_1 = 0.0548$ , $wR_2 = 0.1329$

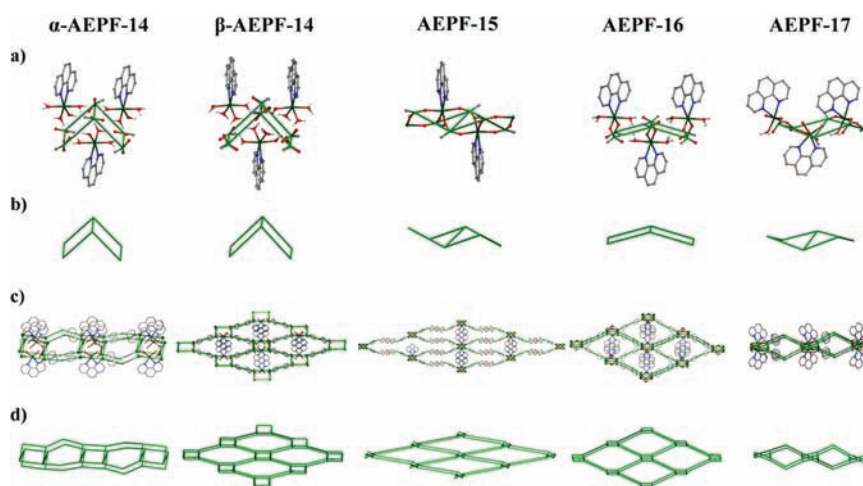


**Figure 2.** Summary of the topological features of compounds AEPF-14 ( $\alpha$ - and  $\beta$ -phases), AEPF-15, AEPF-16, and AEPF-17. (a) Simplification points performed to describe the inorganic SBUs and (b) simplified inorganic SBUs. (c) Simplification points performed to describe the nets and (d) simplified nets for the five compounds.

solvothermal conditions, respectively. The monoclinic  $\alpha$ -AEPF-14 polymorph crystallizes in the  $P2_1/c$  space group, and the orthorhombic  $\beta$ -AEPF-14 crystallizes in the  $Pnna$  space group. A summary of the structure parameters for both polymorphs is shown in Table 3.

In both AEPF-14 polymorphs, the  $Mg^{2+}$  ion is hexacoordinated to four oxygen atoms of water molecules and two nitrogen atoms coming from one phen ligand, to form distorted  $MgN_2O_4$  octahedra. These inorganic polyhedra, which can be considered as inorganic primary building units (PBUs), do not comprise thus, oxygen atoms of the  $L^{2-}$  carboxylate groups. In both cases, hydrogen bonds between coordinated water molecules and  $L^{2-}$  carboxylate groups govern the supramolecular interactions. However, while in  $\alpha$ -AEPF-14 eight different kinds of strong hydrogen bonds were determined, in  $\beta$ -AEPF-14 there are only three of them. To clarify this point, which is crucial to understand the supramolecular features that make the difference between the two polymorphs, hydrogen bond distances and angles for both AEPF-14 compounds were analyzed in detail and presented in Table S6 (Supporting Information). When taking into account these interactions,  $MgN_2O_4$  polyhedra are hydrogen bridged via carboxylate oxygen atoms, giving rise to  $(-Mg-O\cdots O-C-O\cdots O-Mg-)_{\infty}$

inorganic chains parallel to the  $b$  and  $a$  axes for  $\alpha$ - and  $\beta$ -polymorphs, respectively (Figure 1a). In both cases the inorganic chains are hydrogen linked to each other via complete  $L^{2-}$  linker. Nevertheless, while in  $\alpha$ -AEPF-14 each chain is joint to the other two in a 2D way, in  $\beta$ -polymorph a 3D net comes up, as a consequence of a higher number of connections (four in this case) among chains (Figure 1b). The  $\beta$ -AEPF-14 depicted features, together with the presence of  $\pi$ - $\pi$  stacking interaction among the  $L^{2-}$  aromatic rings (distances among centroids 3.655 Å), create a more compact structure, in which there is not any accessible free space. In  $\alpha$ -polymorph, with a 2D supramolecular net and absence of  $\pi$ - $\pi$  interaction, a 4.6% free space ( $140.4$  Å<sup>3</sup> per unit cell) was determined by PLATON (cavity routine).<sup>9</sup>

To consider topological features of AEPF-14 polymorphs, the simplifications of their supramolecular networks were performed, taking into account an interesting work of Yaghi and O'Keeffe,<sup>21</sup> in which the authors carefully studied the rod-packing phenomenon in MOFs. Thus, by considering the infinite  $(-Mg-O\cdots O-C-O\cdots O-Mg-)_{\infty}$  rods found in both AEPF-14 polymorphs as the inorganic secondary building units (SBUs) (the carboxylate was simplified as O-C-O), the two nets then can be simplified in an elegant way (Figure 2a,b).

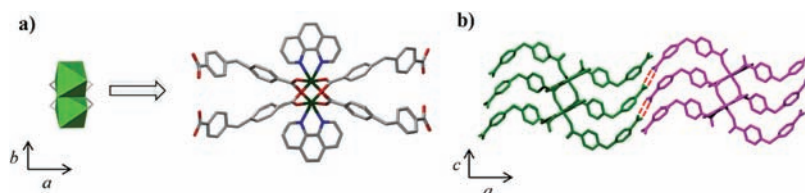


**Figure 3.** (a) Depiction along the *b* axis of the very decorated SBUs built as an extension of the inorganic chains. (b) Two AEPF-15 decorated SBUs hydrogen bounded via the linker carboxylic groups.

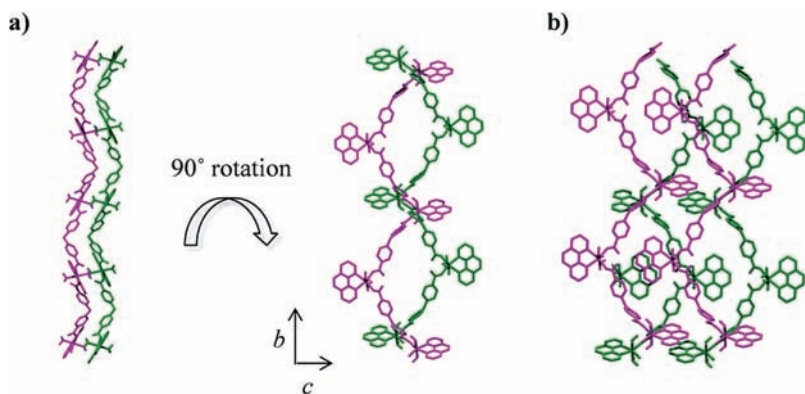


**Figure 4.** AEPF-16 supramolecular framework built up via hydrogen bonds. (a) Double  $[M-L]_{\infty}$  helical covalent chain, showing different orientations. (b) Junction of two double  $[M-L]_{\infty}$  helical chains along the *c* axis.

Taking into account these topological considerations, these SBUs can be described as “ladders” formed by sharing opposite edges of quadrangles. Regarding the  $\alpha$ -AEPF-14 supramolecular framework, these SBUs are linked with the rungs in parallel “parallel rung ladders” to form a uninodal four-connected 2D *sql* net (point symbol  $(4^4.6^2)$ ) (the nodes are located on C atoms of the linker carboxylate groups). However, in the case of the  $\beta$ -AEPF-14 compound, as was mentioned before, each rod is linked to four others, giving rise to a three-dimensional net. Thus, the parallel connection of the rungs in this compound is made in a different way giving rise to a uninodal four-connected 3D *sra* net, whose nodes also correspond to C atoms of the linker carboxylate groups. The main simplification points, as well as the final simplified nets for both AEPF-14 polymorphs, are shown in Figure 2c,d.

**AEPF-15.** The hydrothermal reaction between  $H_2L$  and magnesium acetate tetrahydrate, using phen as chelating ligand, has also given rise to the  $[Mg(HL)_2(phen)]$  compound (AEPF-15), in which the organic linker remains half protonated as the  $HL^-$  anion. AEPF-15 crystallizes in the monoclinic crystal system ( $C2/c$  space group) (see Table S6, Supporting Information, for all parameters).

In AEPF-15 the  $MgN_2O_4$  octahedral PBU is formed by  $Mg^{2+}$  coordination to four oxygen atoms coming from  $HL^-$  carboxylate groups and the two nitrogen atoms of the chelating phen molecule. Linkages of the later form inorganic chains (SBUs) along the *c* axis, through the carboxylate group that acts in a  $\eta^2\mu_2$  coordination mode (Figure 1b). As in this compound the linkers are only covalently bonded to the Mg ions by the deprotonated carboxylate groups, they hang from the PBUs, giving rise to very decorated SBUs (Figure 3a). Typical hydrogen bonds between  $HL^-$  carboxylic acids (Figure 3b and in the Supporting Information Table S7) give rise to the formation of a three-dimensional supramolecular net (Figure 1b).

Concerning the topology of the supramolecular net determined for AEPF-15, the inorganic PBUs are connected to each other through the  $\eta^2\mu_2$  coordinated carboxylate groups, giving rise to  $(-Mg-O-C-O-Mg-)_{\infty}$  rods<sup>21</sup> considered as SBUs. By simplification of these SBUs, one type of four-connected node comes up, which is situated in the carboxylate group C atoms (Figure 2a,b). Thus, the SBU appears as in the former compounds as ladders, but in this case, and probably due to the fact that the linker is directly coordinated to the metal in a bridging way, the rungs are at an angle to each other, so we call them “twisted ladders” (Figure 1b). Through linkages among them via hydrogen bond interactions, a 3D *irl* supramolecular net is built (point symbol  $(4^2.6^3.8)$ ) (Figure 2c,d).

**AEPF-16.** As it was mentioned above in the Synthesis Procedures section, when the pH of the reaction mixture is slightly increased under certain hydrothermal conditions, the novel compound  $[Mg(H_2O)_2(L)(phen)]$  (AEPF-16) is isolated as pure phase. This material crystallizes in the orthorhombic crystal system (*Pnna* space group) (Table S6, Supporting Information). In AEPF-16,  $Mg^{2+}$  ions are coordinated to two oxygen atoms coming from  $L^{2-}$  carboxylate groups, two oxygen atoms of water molecules and the two phen nitrogen atoms giving the  $MgN_2O_4$  octahedral PBU. These PBUs are covalently bonded through the deprotonated  $L^{2-}$  ligand, which acts in a  $\eta^1-\eta^1$  coordination mode, leading to the formation of 1-D polymeric helical chains  $[M-L]_{\infty}$  (Figure 4a). The supramolecular interactions in this compound are governed by three different hydrogen bonds, which are determined between coordination water molecules and  $L^{2-}$  carboxylate groups. The distances and angles of these interactions are listed in Table S8, Supporting Information. If these hydrogen bonds are taken into account, the  $MgN_2O_4$  PBUs are additionally hydrogen bridged via  $L^{2-}$  carboxylate groups, giving rise to  $(-Mg-O\cdots O-C-O\cdots O-Mg-)_{\infty}$  inorganic chains (Figure 1a). The AEPF-16 supramolecular net consists of double helical  $[M-L]_{\infty}$  chains, parallel to the *b* axis, joint among them, via hydrogen bonds in the

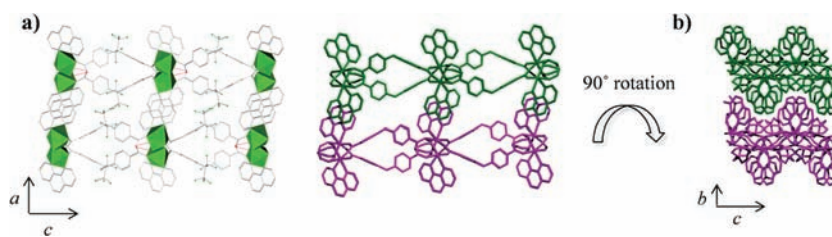


**Figure 5.** (a) Polyhedral view of two layers in AEPF-17 layers viewed along the  $b$  axis and detail of the inorganic chains, showing the hydrogen bonds in red. (b) Depiction of two undulated layers in AEPF-17 viewed along the  $a$  axis.

$c$  direction (Figure 4). The result is a three-dimensional supramolecular framework (Figure 1a).

To consider topological features of AEPF-16, the  $(-\text{Mg}-\text{O}\cdots\text{O}-\text{C}-\text{O}\cdots\text{O}-\text{Mg}-)$  $_{\infty}$  inorganic chains were described as rods<sup>21</sup> (SBUs). By their simplification, only one type of four-connected node appears, which corresponds to the C atoms of carboxylate groups (Figure 2a,b). Then, as occurs in AEPF-14 polymorphs, the SBU consists of rods sharing opposite edge quadrangles named “parallel rung ladders” (Figure 2b). Covalent joints of these ladders through the whole  $\text{L}^{2-}$  linker give rise to a 3D *sra* net. The main simplification points as well as the final simplified net for AEPF-16 are shown in Figure 2c,d.

**AEPF-17.** Finally, under solvothermal conditions, a novel compound with formula  $[\text{Mg}(\text{H}_2\text{O})(\text{L})(\text{phen})]$  (AEPF-17) is obtained as a pure phase. AEPF-17 crystallizes in the orthorhombic crystal system (*Pbca* space group) (Table S6, Supporting Information). The  $\text{Mg}^{2+}$  ions are bonded to three oxygen atoms coming from  $\text{L}^{2-}$  carboxylate groups, one water molecule and two phen nitrogen atoms. These PBUs are connected to each other through the  $\eta^2\mu_2$  coordinated carboxylate groups, giving rise to  $(-\text{Mg}-\text{O}-\text{C}-\text{O}-\text{Mg}-)$  $_{\infty}$  inorganic chains parallel to the  $b$  axis (Figure 1b). Additional intrachain hydrogen bonds are found, due to the presence of coordinated water molecules and carboxylate groups that act in a  $\eta^1$  mode. The distances and angles of these hydrogen bonds are listed in Table S9, Supporting Information. It is worth mentioning that the presence of  $\pi$ - $\pi$  stacking interactions is found among phen rings, with a distance among centroids of 3.743 Å.

In AEPF-17, each inorganic chain described above is bonded to two others via the  $\text{L}^{2-}$  linker, giving rise to undulated layers perpendicular to the  $a$  axis (Figure 5). The described hydrogen bonds do not increase the net dimensionality since they are between the intra chains.

Concerning the topology of AEPF-17 net, as was done before, the inorganic SBUs  $(-\text{Mg}-\text{O}-\text{C}-\text{O}-\text{Mg}-)$  $_{\infty}$  were simplified as rods,<sup>21</sup> giving rise to one type of four-connected nodes, situated in the carboxylate group C atoms (Figure 2a,b). In doing that, the SBU appears also as “twisted ladders” (Figure 1b). Covalent bonding among them via the linker results in a 2D *sql* net (point symbol  $(4^4.6^2)$ ) (Figure 2c,d).

**X-ray Powder Diffraction Studies.** X-ray diffraction data were analyzed by Pawley<sup>10</sup> refinements methodology, using Materials Studio software.<sup>11</sup> For those compounds that have been isolated after optimizing the synthesis procedures, these structural studies have shown the presence of a unique crystalline phase, demonstrating the purity of the bulk samples. Pawley refinement profiles and the main refinement values for AEPF-14 ( $\alpha$ - and  $\beta$ -), AEPF-16, and AEPF-17 are shown in Figures S6–S9 and Tables S11–S14 in the Supporting Information.

### Structural Stability Studies: Theoretical Calculations.

The use of theoretical calculations as a complement in the determination of the factors that govern the mechanisms of MOFs formation processes has been proved to be very useful.<sup>22–26</sup> In order to determine the structural stability of the magnesium frameworks presented in this work and to deepen the understanding of their formation pathways, a series of theoretical DFT plane-wave based calculations were carried out. The apparent formation energies for the studied compounds were obtained by using the VASP package.<sup>15,16</sup> In all cases, the geometry optimization converged to a stable structure with the same topology as that determined experimentally, even though no symmetry constraints were imposed.

On one hand, the polymorphism phenomenon found for the AEPF-14 compound was analyzed in detail by using computational studies. With that purpose, the relative energies for the two AEPF-14 phases ( $\alpha$ - and  $\beta$ -) were determined by DFT-based calculations. As is shown in Figure 6, after comparing the

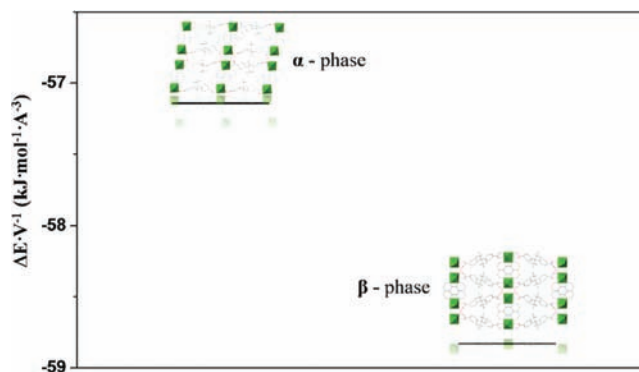


**Figure 6.** Relative energies per volume for both AEPF-14 polymorphs ( $\alpha$ - and  $\beta$ -phases).

relative energies per volume for both structures, it can be concluded that the  $\beta$ -phase is the most stable one. This fact is in good agreement with the higher dimensionality of the supramolecular net of this polymorph (3D) and with the obtained results in the synthesis procedure.

In addition, in order to correlate the structural stability with the synthesis procedures, a series of computational studies were performed to determine the formation energies ( $E_{\text{Formation}}$ ) for those compounds that coexist under certain conditions (Figure 7).

Regarding the hydrothermal reactions performed at lower temperatures ( $T = 160$ – $170$  °C) and short reaction times (1 h to 2 days) (Figure 7A), the coexistence of  $\alpha$ -AEPF-14, AEPF-15, and AEPF-16 compounds has been observed. In addition, the ratio among the phases varies through the time. Thus, while at 160 °C  $\alpha$ -AEPF-14 is the principal component, when shorter reaction times are used, AEPF-15 and AEPF-16 become the

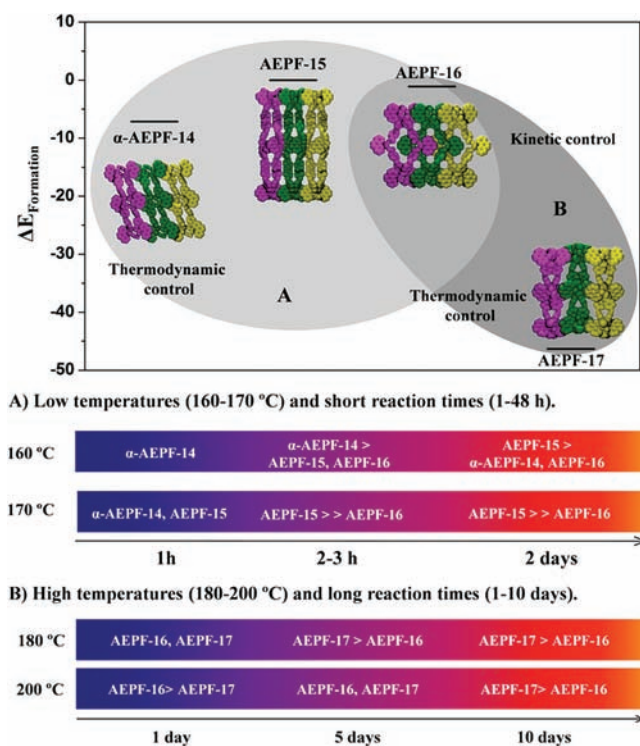


**Figure 7.** (Top) Calculated formation energies ( $\Delta E_{\text{Formation}}$ ) for  $\alpha$ -AEPF-14, AEPF-15, AEPF-16, and AEPF-17 compounds. (Bottom) Scheme of the experimentally determined phases' formation under soft reaction conditions (A) and hard reaction conditions (B).

principal components of the products mixture for longer reaction times. Taking into account the results coming from formation energies (Figure 7), several conclusions can be drawn. First,  $\alpha$ -AEPF-14 presents the lowest  $E_{\text{Formation}}$  among these three phases, which seems to indicate that, at shorter reaction times, thermodynamic processes govern the reaction. However, with the increase in reaction time and temperature (170 °C), the reaction obeys a kinetic control, which leads to the formation of the less stable phases (AEPF-15 and AEPF-16).

Concerning the hydrothermal reactions performed at higher temperatures ( $T = 180$  and  $200$  °C) and long reaction times (1–10 days) (Figure 7B), the coexistence of AEPF-16 and AEPF-17 compounds has been observed. Moreover, the ratio among the phases varies through the time. Thus, at 180 °C, after 1 day of reaction, AEPF-16 and AEPF-17 are found in a similar proportion; with the increase of the reaction temperature, AEPF-16 becomes the major component of the products mixture. In addition, the use of longer reaction times leads to the formation of AEPF-17 as a principle phase. Taking into the

obtained  $E_{\text{Formation}}$  values for these compounds (Figure 7), it can be suggested that a competition between both thermodynamic and kinetic processes takes place under these conditions. However, when longer reaction times are used, the more stable AEPF-17 compound is mainly obtained (thermodynamic control). At 200 °C, an increase of the kinetically controlled phase (AEPF-16) is observed.

**Dehydration Processes: AEPF-14 Polymorphs and AEPF-16.** As was mentioned above, both  $\beta$ -AEPF-14 and AEPF-16 compounds exhibit 3D supramolecular nets that belong to the sra topological type. On the other hand, they present the same Mg:phen:L ratio per molecular formula, but different numbers of coordinated water molecules per metal ion. In this context, we were interested in studying the dehydration processes of these compounds, in order to elucidate some common structural changes during the loss of their coordinated water molecules. This study was also extended to the  $\alpha$ -AEPF-14 compound, to determine the possible structural transformations between both AEPF-14 polymorphic forms.

Taking into account TGA results (see the Supporting Information, Section S4), both AEPF-14 samples were heated under vacuum to ensure the removal of coordination water molecules ( $\alpha$ -AEPF-14 at 150 °C and  $\beta$ -AEPF-14 at 180 °C). The dry samples were examined by PXRD in order to determine the structural changes provoked by the dehydration. Although for both polymorphs an important loss of crystallinity was detected after this heating treatment, the indexation of their PXRD patterns could be performed by using DICVOL04<sup>27,28</sup> software, implemented in the FullProf package.<sup>29</sup> In addition, in order to compare the obtained results, the same study was performed with AEPF-16 compound (the sample was heated at 150 °C). The cell parameters found for the dry samples, together with those determined by single crystal X-ray diffraction for the as-synthesized compounds, are shown in Table 4.

Taking into account these results, several conclusions can be drawn. Regarding the behavior of AEPF-16 during the dehydration process, the compound suffers an isotropic contraction ( $\sim 1.5\%$ ) of its cell parameters, giving rise to a reduction of 4.3% in its cell volume ( $V_{\text{AEPF-16}} = 2808.1 \text{ \AA}^3$ ,  $V_{\text{dryAEPF-16}} = 2686.8 \text{ \AA}^3$ ) (Table 4), retaining the orthorhombic crystal system and its crystallinity.

In the case of AEPF-14, both polymorphs exhibit different structural transformations when losing their coordinated water molecules, probably due to different topologies found in their supramolecular nets. Thus, while  $\beta$ -polymorph exhibits double helical chains joint along the  $a$  and the  $c$  axes via hydrogen bonds (sra net), for  $\alpha$ -polymorph only undulating double chains joint along the  $b$  axis can be found (sql layers). As is

**Table 4.** A Summary the Cell Parameters for AEPF-14 ( $\alpha$ - and  $\beta$ -) and AEPF-16 As-Synthesised (Found by Single Crystal X-ray Diffraction) and after the Dehydration Process (Found by PXRD)

	$\alpha$ -AEPF-14	dry $\alpha$ -AEPF-14	$\beta$ -AEPF-14	dry $\beta$ -AEPF-14	AEPF-16	dry AEPF-16
$a/\text{\AA}$	13.2022(2)	11.00(11)	7.3064(2)	6.406(8)	9.3105(3)	9.1736(8)
$b/\text{\AA}$	7.6135(1)	9.11(2)	32.6024(10)	27.404(24)	26.8940(8)	26.488(5)
$c/\text{\AA}$	31.0128(5)	27.52(4)	12.5442(4)	11.745(12)	11.2146(3)	11.057(3)
$\alpha/\text{deg}$	90.0	90.0	90.0	90.0	90.0	90.0
$\beta/\text{deg}$	99.863(1)	97.6(7)	90.0	90.0	90.0	90.0
$\gamma/\text{deg}$	90.0	90.0	90.0	90.0	90.0	90.0
$V/\text{\AA}^3$	3071.18(8)	2735.25	2988.11(16)	2062.01	2808.10(14)	2686.82
figures of merit		$M_{12} = 12, F_{12} = 19$		$M_{14} = 10, F_{14} = 12$		$M_{20} = 35, F_{20} = 68$

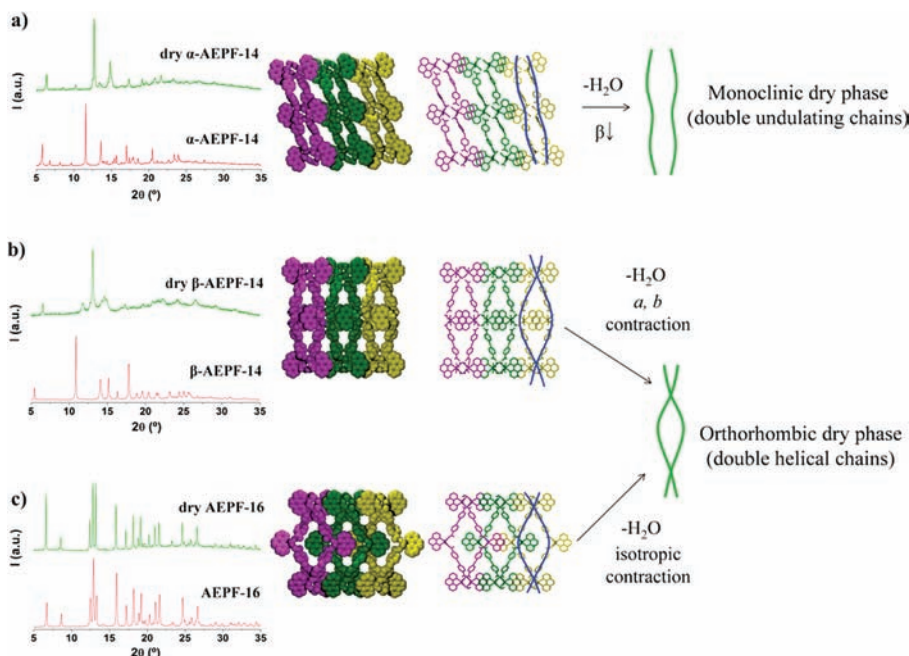


**Figure 8.** Structural study performed with dehydrated samples for (a)  $\alpha$ -AEPF-14, (b)  $\beta$ -AEPF-14, and (c) AEPF-16. On the left, comparisons of PXRD patterns before and after the dehydration treatment are shown. On the right, stick and space filling representations of the double chain structures are depicted.

shown in Table 4, after dehydration the orthorhombic  $\beta$ -polymorph retains its crystal symmetry although it suffers an important contraction of the  $b$  axis ( $\sim 16\%$ ) (along which the  $2_1$  axis runs) and the  $a$  axis ( $\sim 12\%$ ) (along which the  $\pi$ - $\pi$  stacking runs). These results point out the first conclusion: the similarities found between the cell parameters of **dry  $\beta$ -AEPF-14** and **dry AEPF-16** allow us to elucidate a transformation of both compounds to a similar orthorhombic phase with a double helical chain structure (Figure 8b,c). Considering the topological similarities between the two compounds, the structural transformation caused by the loss of coordinated water molecules can be explained as a subtle contraction of this 1D helical structure.

In the case of the **dry  $\alpha$ -AEPF-14** compound, its PXRD pattern was indexed to a monoclinic cell, which exhibits similar cell parameter values to those of dry AEPF-16 but a value of  $\beta$  of  $\sim 98^\circ$ , which is far from the orthorhombic crystal system (Table 4). So, the second conclusion that can be drawn is the following: starting from  $\alpha$ -monoclinic polymorph, in which the double chains are not joint via interchain hydrogen bonds, the formation of the 1D helical structure does not take place (Figure 8a). Thus, the structural transformation that suffers  $\alpha$ -AEPF-14 after the dehydration treatment can be caused by little changes in the undulating packing of these double layers.

## CONCLUSIONS

In summary, the effect of introducing of N-donor chelating ancillary ligands on the synthesis of Mg MOFs has been explored, resulting in five new compounds, which exhibit 0D, 1D, and 2D dimensionalities, and 2D and 3D supramolecular frameworks: a molecular magnesium material with polymorphism (named AEPF-14,  $\alpha$ - and  $\beta$ -phases), a 1D MOF (AEPF-15), a 1D helical MOF (AEPF-16), and a 2D MOF (AEPF-17). The role that the synthesis conditions play in the formation of each phase has been exhaustively studied and complemented with theoretical calculations. Taking into account both the results of the synthesis

and the relative formation energies for the compounds that coexist under certain hydrothermal conditions, the thermodynamic or kinetic control of the reaction have been established.  $\alpha$ -AEPF-14 can be regarded as the precursor, in which  $\text{Mg}^{2+}$  ions are coordinated, besides to the blocking ligand, only to water molecule oxygen atoms. When reaction time goes on, it gets dissolved, and then the less stable phases, AEPF-15 and AEPF-16, whose Mg coordination spheres comprise carboxylate oxygen atoms, energetically compete to come up in a kinetically controlled process. The energetically more stable AEPF-17 appears at higher temperature and much longer reaction time, the process being thus thermodynamically controlled.

Considering structural and topological features, hydrogen bonds govern the supramolecular interactions in the five compounds, achieving uninodal four-connected supramolecular nets with higher dimensionality in all the cases except for AEPF-17, where the chelating ligands hinder any interlayer hydrogen bond interaction. In those cases in which O-C-O covalent bridges join the inorganic polyhedra to form the SBU in the rod packing simplification, the later results in a "twisted ladder", while in those compounds in which the linkage among polyhedra is made only via hydrogen bonds the SBU is a regular "parallel rung ladder".

In addition, the AEPF-14 polymorphism was studied in detail, determining that  $\beta$ -polymorph being the most stable, only can be obtained via solvothermal synthesis in a media in which one-third of water was substituted by acetone in volume.

Finally, the dehydration studies performed on AEPF-14 ( $\alpha$ - and  $\beta$ -) and AEPF-16 have shown that the topology of their supramolecular networks determines the structural changes that take place during the dehydration processes of these Mg compounds.

## ASSOCIATED CONTENT

### Supporting Information

Synthetic procedures, structural analyses by single crystal X-ray diffraction, powder X-ray diffraction, infrared spectroscopy, and

thermal gravimetric analyses, along with ORTEP representations for these crystal structures shown in Figures S1–S5. This material is available free of charge via the Internet at <http://pubs.acs.org>.

## AUTHOR INFORMATION

### Corresponding Author

\*amonge@icmm.csic.es

### Notes

The authors declare no competing financial interest.

## ACKNOWLEDGMENTS

This work has been supported by the Spanish MICINN Projects MAT2010-17571, MAT2009-09960, CTQ 2007-28909-E/BQU, CAM: S2009/MAT-1756/CAM, and Consolider-Ingenio CSD2006-2001. A.E.P.P. acknowledges a JAE fellowship from CSIC and Fondo Social Europeo from EU. V.A.P.O. acknowledges financial support from the MCYT in the Ramon y Cajal Program and ENE2009-09432. Computational time has been provided by the Centre de Supercomputació de Catalunya (CESCA) and Centro de Supercomputación de Galicia (CESGA) by generous grants.

## REFERENCES

- (1) (a) Fromm, K. M. *Coord. Chem. Rev.* **2008**, *252*, 856. (b) Banerjee, D.; Parise, J. B. *Cryst. Growth Des.* **2011**, DOI: 10.1021/cg2008304.
- (2) (a) Dincă, M.; Long, J. R. *J. Am. Chem. Soc.* **2005**, *127*, 9376. (b) Platero-Prats, A. E.; de la Peña-O'Shea, V. A.; Snejko, N.; Monge, Á.; Gutiérrez-Puebla, E. *Chem.—Eur. J.* **2010**, *16*, 11632. (c) Mallick, A.; Saha, S.; Pachfule, P.; Roy, S.; Banerjee, R. *Inorg. Chem.* **2011**, *50*, 1392.
- (3) Platero-Prats, A. E.; de la Peña-O'Shea, V. A.; Iglesias, M.; Snejko, N.; Monge, Á.; Gutiérrez-Puebla, E. *ChemCatChem* **2010**, *2*, 147.
- (4) Gándara, F.; de la Peña-O'Shea, V. A.; Illas, F.; Snejko, N.; Proserpio, D. M.; Gutiérrez-Puebla, E.; Monge, M. A. *Inorg. Chem.* **2009**, *48*, 4707.
- (5) Platero-Prats, A. E.; Iglesias, M.; Snejko, N.; Monge, Á.; Gutiérrez-Puebla, E. *Cryst. Growth Des.* **2011**, *11*, 1750.
- (6) Bruker SAINTplus package. Bruker AXS Inc.: Madison, Wisconsin, USA, 2006.
- (7) Sheldrick, G. M. SADABS program integrated in SAINTplus package. Bruker AXS Inc.: Madison, Wisconsin, USA.
- (8) Bruker SHELXTL package. Bruker AXS Inc.: Madison, Wisconsin, USA, 2006.
- (9) Spek, A. L. PLATON, A multipurpose Crystallographic Tool; Utrecht University: Utrecht, Holland, 2005.
- (10) Pawley, G. S. *J. Appl. Crystallogr.* **1981**, *14*, 357.
- (11) Materials Studio Modelling 4.4, [http://www.accelerys.com/mstudio/ms\\_modeling](http://www.accelerys.com/mstudio/ms_modeling)
- (12) Blatov, V. A. *IUCr Comput. Comm. Newsllett.* **2006**, *7*, 4, see also <http://www.topos.ssu.samara.ru>.
- (13) Alexandrov, E. V.; Blatov, V. A.; Kochetkov, A. V.; Proserpio, D. M. *CrystEngComm* **2011**, *13*, 3947.
- (14) O'Keeffe, M.; Yaghi, O. M. *Chem. Rev.* **2012**, *112*, 675–702.
- (15) Kresse, G.; Furthmüller, J. *Comput. Mater. Sci.* **1996**, *6*, 15.
- (16) Kresse, G.; Hafner, J. *Phys. Rev. B* **1993**, *47*, 558.
- (17) Perdew, J. P.; Wang, Y. *Phys. Rev. B* **1992**, *45*, 13244.
- (18) Perdew, J. P.; Chevary, J. A.; Vosko, S. H.; Jackson, K. A.; Pederson, M. R.; Singh, D. J.; Fiolhais, C. *Phys. Rev. B* **1992**, *46*, 6671.
- (19) Blochl, P. E. *Phys. Rev. B* **1994**, *50*, 17953.
- (20) Kresse, G.; Joubert, D. *Phys. Rev. B* **1999**, *59*, 1758.
- (21) Rosi, N. L.; Kim, J.; Eddaoudi, M.; Chen, B.; O'Keeffe, M.; Yaghi, O. M. *J. Am. Chem. Soc.* **2005**, *127* (5), 1504.

- (22) Lee, C.; Mellot-Draznieks, C.; Slater, B.; Wu, G.; Harrison, W. T. A.; Rao, C. N. R.; Cheetham, A. K. *Chem. Commun.* **2006**, *25*, 2687.
- (23) Bernini, M. C.; de la Peña-O'Shea, V. A.; Iglesias, M.; Snejko, N.; Gutiérrez-Puebla, E.; Brusau, E. V.; Narda, G. E.; Illas, F.; Monge, M. Á. *Inorg. Chem.* **2010**, *49*, 5063.
- (24) Keskin, S.; Liu, J.; Rankin, R. V.; Karl Jhonson, J.; Sholl, D. S. *Ind. Eng. Chem. Res.* **2009**, *48*, 2355 and references therein.
- (25) Coombes, D. S.; Cora, F.; Mellot-Draznieks, C.; Bell, R. G. *J. Phys. Chem. C* **2009**, *113*, 544.
- (26) Sillar, K.; Hofmann, A.; Sauer, J. *J. Am. Chem. Soc.* **2009**, *131* (11), 4143.
- (27) Louër, D.; Louër, M. *J. Appl. Crystallogr.* **1972**, *5*, 271.
- (28) Boulton, A.; Louër, D. *J. Appl. Crystallogr.* **1991**, *24*, 987.
- (29) Rodríguez-Carvajal, J. *Physica B* **1993**, *192*, 55.